Magnetic properties of a spin-$\frac{1}{2}$ mixed coordination lattice

Satoshi Morota [1], Kazuma Toko [1], Takanori Kida [2], Masayuki Hagiwara [2], Koji Araki,[3] Yuko Hosokoshi [1]
Kenta Kimura [4,5], Yoshiki Iwasaki,[5,6] and Hironori Yamaguchi [1,5]

[1]*Department of Physics, Osaka Metropolitan University, Osaka 599-8531, Japan*
[2]*Center for Advanced High Magnetic Field Science (AHMF), Graduate School of Science, Osaka University, Osaka 560-0043, Japan*
[3]*Department of Applied Physics, National Defense Academy, Kanagawa 239-8686, Japan*
[4]*Department of Materials Science, Osaka Metropolitan University, Osaka 599-8531, Japan*
[5]*Innovative Quantum Material Center (IQMC), Osaka Metropolitan University, Osaka 599-8531, Japan*
[6]*Department of Physics, College of Humanities and Sciences, Nihon University, Tokyo 156-8550, Japan*

We successfully synthesized $(p\text{-Py-V})_2[\text{Cu(hfac)}_2]$, a verdazyl-based complex. Molecular orbital calculations revealed that three antiferromagnetic (AF) exchange interactions form a spin-$\frac{1}{2}$ lattice with coordination numbers 2 and 4. The magnetic susceptibility and specific heat exhibit contributions of AF correlations and a phase transition to an AF ordered state at $T_N = 3.6$ K. The magnetization curve exhibits an almost linear increase in the low-field region for $T > T_N$. Furthermore, we observe a nonlinear increase in the high-field region, demonstrating the magnetic moment reduction caused by the strong quantum fluctuations. Through numerical analysis, we reveal a hump structure of magnetic susceptibility and a 1/3 magnetization plateau that emerge owing to the effective spin state. These results provide a model compound forming a spin-$\frac{1}{2}$ mixed coordination lattice and an understanding of its unique quantum properties attributed to strong quantum fluctuations.

I. INTRODUCTION

Quantum fluctuations in spin lattices are fundamental to understanding quantum properties in condensed-matter systems. Honeycomb lattice composed of hexagonal plaquettes exhibits a smaller coordination number (i.e., 3) than other two-dimensional (2D) spin lattices. Accordingly, it yields increased quantum fluctuations, as fewer neighboring spins result in less stabilization of the spin configuration, allowing for larger deviations and uncertainties in spin states, thus placing it near the quantum critical limit. Although antiferromagnetic (AF) honeycomb lattices exhibit an ordered ground state with a bipartite structure, strong quantum fluctuations reduce the magnetic moment per site. Therefore, the ground state is vulnerable [1–4]. Modulations, such as distortion [5–7], randomness [8], and anisotropy [9], in the exchange interactions that form a honeycomb lattice can easily destroy the ordered state. This results in the formation of exotic quantum states. The Kitaev model, which forms a honeycomb lattice with bond-dependent anisotropic interactions, has attracted considerable attention regarding quantum spin liquid hosting fractionalized Majorana fermion excitations [10,11]. If the coordination number of a honeycomb lattice increases by one (i.e., 4) in a 2D system, it corresponds to a square lattice. The discovery of high-temperature superconductors in layered cuprates has motivated studies of the AF square lattice as the parent spin system. Although the ground state is a bipartite structure similar to a honeycomb lattice, the quantum fluctuations reduce the magnetic moment per site and cause renormalization of the spin wave energy [12,13]. The mixed coordination lattice, characterized by coordination

numbers 2 and 4, is the focus of this study. Although this lattice is composed of square and hexagonal plaquettes, the coordination number of the hexagonal plaquettes is lower than that of conventional lattices. Given the involvement of two different topologies and the small coordination number, unique quantum properties are expected to emerge due to the effects of strong quantum fluctuations. However, there have been no prior studies, either experimental or theoretical, on the 2-4-coordinated lattice, making it a promising area for discovering interesting phenomena.

Advanced spin-lattice designs can be generated from the modulation of the molecular structures of organic radicals. Utilizing the divers molecular structures of triphenyl verdazyl radicals, we develop verdazyl-based quantum organic material (V-QOM) and demonstrate the realization of unconventional spin lattices yet to be realized in conventional inorganic materials [14–18]. Furthermore, we expand V-QOM by combining it with $3d$ transition metals. This combination results in the formation of spin lattices comprising intramolecular π-d coupling and intermolecular π-π stacking [19–22]. Moreover, the metal-radical coupling, magnetic anisotropy, and spin size in these complexes are inherent to the metallic elements and are involved in the formation of spin lattices. Because the metal atoms in these complexes are coordinated to two radical ligands, each molecule contains three interacting spins, providing effective coupling units for the formation of spin lattices with a small coordination number of 2.

In a previous study, we demonstrated the realization of mixed coordination lattices using V-QOM. For $(p\text{-Py-V-}p\text{-F})_2[\text{Ni(hfac)}_2]$ [23], we observed the formation of a spin-$(\frac{1}{2}, 1)$ 2-4-coordinated lattice. The magnetization curve

displayed a 1/2 plateau, representing the full polarization of spin-1, forming an effective AF chain. An effective spin-$\frac{1}{2}$ ladder can explain the magnetic behavior after the 1/2 plateau. In $(p\text{-Py-V-}p\text{-F})_2[\text{Co(hfac)}_2]$ [24], the 2-4-coordinated lattice is composed of spin-$\frac{1}{2}$ on the radical and fictitious spin-$\frac{1}{2}$ on the Co^{2+} ion with Ising-like exchange interactions originating from the spin-orbit coupling of the Co^{2+} ion. Paramagnetic behavior associated with the Co spins, and a 3/5 plateau was observed, demonstrating a rung-singlet-like ground state in the effective ladder composed of radical spins with fully polarized Co spins. The peculiar behavior of the linear magnetization curve after the magnetization plateau indicates a quantum phase transition from the gapped quantum state to the 2D magnetic state. These results demonstrate that V-QOM is effective for forming 2-4-coordinated lattices with various topologies. Furthermore, the magnetic properties of the 2-4-coordinated lattices reflect strong quantum fluctuations, resulting in unconventional quantum behavior.

In this study, we synthesized $(p\text{-Py-V})_2[\text{Cu(hfac)}_2]$ (p-Py-V = 3-(4-pyridinyl)-1,5-diphenylverdazyl, hfac = 1,1,1,5,5,5-hexafluoro-2,4-pentanedione), which is a verdazyl-Cu complex. Molecular orbital (MO) calculations indicated that the three types of exchange interactions form a spin-$\frac{1}{2}$ 2-4-coordinated lattice. At $T_N = 3.6$ K, the magnetic susceptibility and specific heat exhibit a phase transition to an AF ordered state. For $T > T_N$, the magnetization curve exhibits an almost linear increase in the low-field region. Furthermore, a nonlinear increase is observed in the high-field region, which demonstrates a reduction of the magnetic moment caused by the strong quantum fluctuations. Numerical analysis revealed the quantum behavior attributed to the topology of a 2-4-coordinated lattice.

II. EXPERIMENT

We synthesized p-Py-V via the conventional procedure for producing the verdazyl radical [25]. A solution of $\text{Cu(hfac)}_2 \cdot 2\text{H}_2\text{O}$ (429.9 mg, 0.90 mmol) in 2 ml ethanol and 10 ml of heptane was refluxed at 60 °C. A solution of p-Py-V (282.0 mg, 0.90 mmol) in 5 ml of CH_2Cl_2 was slowly added and stirred for 1 h. After the mixed solution was cooled to room temperature, a dark-green crystalline solid of $(p\text{-Py-V})_2[\text{Cu(hfac)}_2]$ was separated by filtration and washed with heptane. Single crystals were obtained via recrystallization from a mixed solvent of CH_2Cl_2 and methanol at 10 °C.

The x-ray intensity data were collected using a Rigaku XtaLAB Synergy-S instrument. The crystal structures was determined using a direct method using SIR2004 [26] and refined using the SHELXL97 crystal structure refinement program [27]. Anisotropic and isotropic thermal parameters were employed for nonhydrogen and hydrogen atoms, respectively, during the structure refinement. The hydrogen atoms were positioned at their calculated ideal positions. Magnetization measurements were conducted using a commercial superconducting quantum interference device (SQUID) magnetometer (MPMS, Quantum Design). High-field magnetization in pulsed magnetic fields was measured using a non-destructive pulse magnet at AHMF, Osaka University. Specific heat measurements were performed using a commercial calorimeter (PPMS, Quantum Design) employing a thermal relaxation

method. All the experiments utilized small, randomly oriented single crystals.

Molecular orbital (MO) calculations were performed using the UB3LYP method as broken-symmetry hybrid density functional theory calculations with the basis sets of 6-31G(d, p). All calculations were performed using the GAUSSIAN09 software package. The convergence criterion was set at 10^{-8} hartree. We employed a conventional evaluation scheme to estimate the intermolecular exchange interactions in the molecular pairs [28].

The quantum Monte Carlo (QMC) code is based on the directed loop algorithm in the stochastic series expansion representation [29]. The calculations were performed for $N = 1200$ under the periodic boundary condition, where N denotes the system size. It was confirmed that there is no significant size-dependent effect. All calculations were carried out using the ALPS application [30,31]. To avoid the difficulty of calculations with site-dependent g values, we used a uniform normalized g value. The calculated results were calibrated using the average g value.

III. RESULTS

A. Crystal structure and spin model

The crystallographic parameters of $(p\text{-Py-V})_2[\text{Cu(hfac)}_2]$ are listed in Table I. Figure 1(a) shows the molecular structure of $(p\text{-Py-V})_2[\text{Cu(hfac)}_2]$. In the molecule, the verdazyl radical, p-Py-V, and the Cu^{2+} ion have a spin value of 1/2. The Cu^{2+} ion is coordinated with two p-Py-V ligands, creating an octahedral coordination environment. The two radicals in the molecule are equivalent regarding crystallography owing to the presence of an inversion center at the position of the Cu atom. Table II lists the bond lengths and angles of the Cu atom. Regarding the spin density distribution in the radical, MO calculations revealed that approximately 63% of the total spin density is localized on the central ring consisting of four

TABLE I. Crystallographic data for $(p\text{-Py-V})_2[\text{Cu(hfac)}_2]$.

Formula	$C_{48}H_{34}CuF_{12}N_{10}O_4$
Crystal system	Triclinic
Space group	$P\bar{1}$
Temperature (K)	100
a (Å)	9.6047(5)
b (Å)	9.9262(5)
c (Å)	13.2820(5)
α (degrees)	100.008(4)
β (degrees)	105.183(4)
γ (degrees)	103.823(4)
V (Å³)	1148.32(9)
Z	1
D_{calc} (g cm⁻³)	1.600
Total reflections	2849
Reflection used	2611
Parameters refined	340
R [$I > 2\sigma(I)$]	0.0496
R_w [$I > 2\sigma(I)$]	0.1360
Goodness of fit	1.076
CCDC	2 373 893
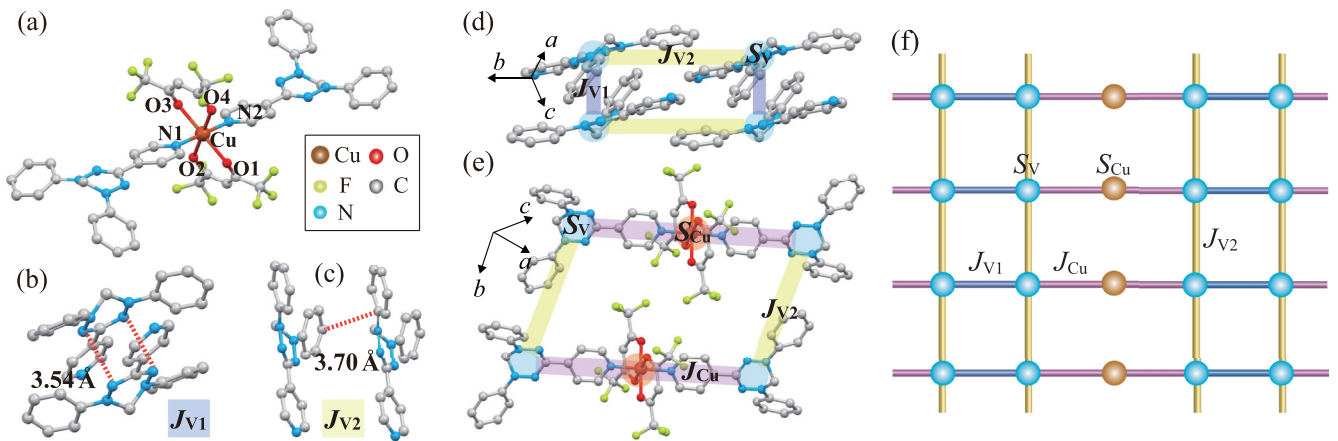
FIG. 1. (a) Molecular structure of $(p\text{-Py-V})_2[\text{Cu(hfac)}_2]$, which causes intramolecular exchange interaction J_{Cu} between radical and Cu spins. The hydrogen atoms have been omitted for clarity. Molecular pairs associated with the exchange interactions of (b) J_{V1} and (c) J_{V2}. The dashed lines indicate N-N and C-C short contacts. (d) Crystal structure forming a square plaquette; each Cu(hfac)$_2$ in the molecule is omitted for clarity. (e) Crystal structure forming a hexagonal plaquette. The blue and brown nodes represent the spin-$\frac{1}{2}$ of the radicals and Cu atoms, respectively. The thick lines represent the exchange interactions, J_{V1}, J_{V2}, and J_{Cu}. (f) Spin-$\frac{1}{2}$ 2-4-coordinated lattice in $(10\bar{1})$ plane.

N atoms. Each phenyl ring directly attached to the central N atom contributes approximately 12–18% of the spin density. The pyridine ring accounts for less than 7% of the spin density. In addition, the MO calculations indicate two primary AF exchange interactions between the radicals with N-N and C-C short contacts, as shown in Figs. 1(b) and 1(c). Their values were evaluated to be $J_{\text{V1}}/k_B = 24.6$ K and $J_{\text{V2}}/k_B = 3.8$ K, defined within the Heisenberg spin Hamiltonian, given by $\mathcal{H} = J_n \sum_{\langle i,j \rangle} \mathbf{S}_i \cdot \mathbf{S}_j$, where $\sum_{\langle i,j \rangle}$ denotes the sum over neighboring spin pairs. The radical pairs associated with J_{V1} and J_{V2} are related by inversion symmetry and translational symmetry along the b axis, respectively, forming a square plaquette, as shown in Fig. 1(d). For the intramolecular case, the AF exchange interaction between the spin on the radical and Cu atom was evaluated to be $J_{\text{Cu}}/k_B = 41.1$ K. Because MO calculations tend to overestimate the intramolecular interactions between verdazyl radicals and transition metals, we expected the actual values of J_{Cu} to be approximately half of the MO evaluation [20,32]. The spins coupled by J_{V2} and J_{Cu} yield a hexagonal plaquette, as shown in Fig. 1(e). Therefore, the overall connection through J_{V1}, J_{V2}, and J_{Cu} from a spin-$\frac{1}{2}$

2-4-coordinated lattice with two different spin sites, S_{V} and S_{Cu}, as depicted in Fig. 1(f). The molecular arrangement pattern forming the spin lattice is equivalent to that in previous work [23,24].

B. Magnetic and thermodynamic properties

Figure 2(a) shows the temperature dependence of the magnetic susceptibility χ at 0.1 T, indicating a broad peak at

TABLE II. Bond distances (Å) and angles (°) related to the Cu atom for $(p\text{-Py-V})_2[\text{Cu(hfac)}_2]$.

Cu–N1	1.99	O1–Cu–O2	85.5
Cu–N2	1.99	O2–Cu–O3	94.5
Cu–O1	2.27	O3–Cu–O4	85.5
Cu–O2	2.05	O4–Cu–O1	94.5
Cu–O3	2.27	N1–Cu–O4	89.9
Cu–O4	2.05	O4–Cu–N2	90.2
		N2–Cu–O2	89.9
		O2–Cu–N1	90.2
		N1–Cu–O3	88.7
		O3–Cu–N2	91.3
		N2–Cu–O1	88.7
		O1–Cu–N1	91.3
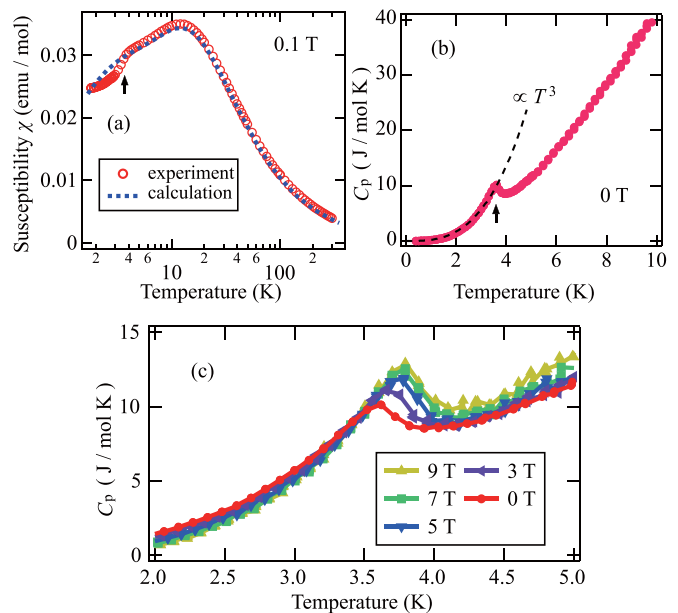
FIG. 2. Temperature dependence of (a) magnetic susceptibility $(\chi = M/H)$ of $(p\text{-Py-V})_2[\text{Cu(hfac)}_2]$ at 0.1 T. The broken line represents the calculated results for the spin-$\frac{1}{2}$ 2-4-coordinated lattice with $\alpha = J_{\text{V1}}/J_{\text{Cu}} = 0.70$ and $\beta = J_{\text{V2}}/J_{\text{Cu}} = 0.15$. (b) Temperature dependence of the specific heat C_p of $(p\text{-Py-V})_2[\text{Cu(hfac)}_2]$ at 0 T. The arrows indicate the phase transition temperature T_N. The broken line shows the T^3 fit below T_N. (c) C_p at various magnetic fields.
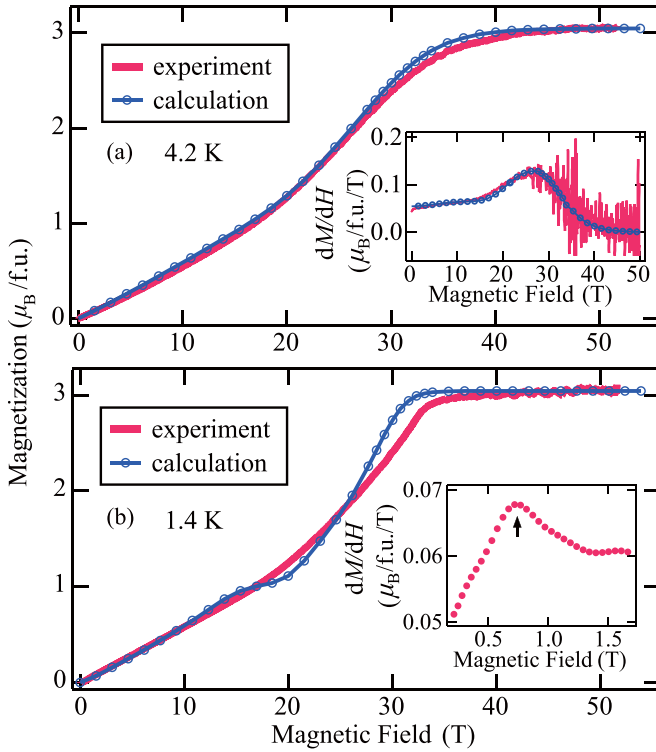
FIG. 3. Magnetization curves of $(p\text{-Py-V})_2[\text{Cu(hfac)}_2]$ at (a) 4.2 K and (b) 1.4 K in pulsed magnetic fields. The solid lines with open circles represent the calculated results for the spin-$\frac{1}{2}$ 2-4-coordinated lattice with $\alpha = J_{V1}/J_{Cu} = 0.70$ and $\beta = J_{V2}/J_{Cu} = 0.15$. The insets show the field derivative of the magnetization curve. The arrow indicates a peak associated with the spin-flop transition.

approximately 13 K. In addition, a discontinuous change was observed at approximately $T_N = 3.6$ K, which can be attributed to a phase transition to a three-dimensional (3D) ordered state owing to weak but finite interplane interactions. The experimental result for the specific heat C_p at zero-field exhibited a sharp peak at T_N, demonstrating the phase transition, as shown in Fig. 2(b). Below T_N, C_p exhibits T^3 dependence, which indicates the contribution from the linear magnon dispersions in the AF 3D ordered state [33,34]. The lattice contribution of the specific heat given by Debye's T^3 law for low-temperature regions has been confirmed to be smaller, $\sim 0.01T^3$, for verdazyl-based compounds [14–16], and thus the observed temperature dependence is attributed to the magnetic contributions in the low-temperature regions. Applying magnetic fields induced a slight increase in T_N, as shown in Fig. 2(c). This field dependence of T_N is predicted for quasi-2D Heisenberg AF systems as a consequence of field-enhanced effective easy-plane anisotropy [35,36]. In 2D systems, quantum fluctuations are significant due to reduced dimensionality, disrupting long-range magnetic order. An external magnetic field reduces these fluctuations by aligning the spins, stabilizing the magnetic order and increasing T_N. This behavior has actually been observed in some model compounds for the spin-$\frac{1}{2}$ quasi-2D system [37,38]. Therefore, the field dependence of the specific heat also evidences the quasi-2D character of the present system.

Figures 3(a) and 3(b) show the magnetization curves under a pulsed magnetic field at 4.2 and 1.4 K, respectively. At both temperatures, the magnetization curve is observed up to saturation. Since the increase of T_N becomes almost unchanged with ~ 3.8 K above 5 T, as shown in Fig. 2(c), the experimental result at 4.2 K corresponds to the paramagnetic behavior above T_N. Based on the isotropic g value (2.0) of organic radicals, a saturation value of 3.05 μ_B/f.u. suggests an average g value of approximately 2.1 for the Cu spin. In the low-field region at 4.2 K, the magnetization curve exhibited an almost linear increase, as shown in the inset of Fig. 3(a). For $T < T_N$, the field derivative of the magnetization exhibited a distinct peak at approximately 0.73 T, as shown in the inset of Fig. 3(b). This indicates a spin-flop transition caused by a minor magnetic anisotropy, which can be described by a classical spin model in the ordered phase [38]. Meanwhile, we observed a nonlinear increase with a concave shape in the high-field region at both temperatures. In typical quantum spin systems, quantum fluctuations are suppressed by applying magnetic fields, resulting in a concave shape of the magnetization curve. Accordingly, the observed behavior suggests that the nonlinear behavior in the high-field region reflects the reduction of the magnetic moment caused by the strong quantum fluctuations.

IV. ANALYSES AND DISCUSSION

Considering the results of the MO calculations, we investigated the magnetic properties based on a spin-$\frac{1}{2}$ 2-4-coordinated lattice composed of the AF interactions J_{V1}, J_{V2}, and J_{Cu}. The magnetic susceptibility and magnetization curve were calculated using the QMC method by considering the parameters $\alpha = J_{V1}/J_{Cu}$ and $\beta = J_{V2}/J_{Cu}$. We note the magnetic susceptibility with the broad peak above T_N and the magnetization curve with the low-field linear and high-field nonlinear increases at 4.2 K as the intrinsic behaviors that originate from correlations in the present spin model. Considering the parameter dependence, good agreement was obtained between the experimental and calculated results using $\alpha = 0.70$ and $\beta = 0.15$ ($J_{Cu}/k_B = 21$ K), as shown in Figs. 2(a) and 3(a). The calculated result successfully reproduced the characteristics of the magnetization curve, including the peak position of dM/dH, as shown in the inset of Fig. 3(a). Meanwhile, the calculated magnetization curve at 1.4 K exhibited a 1/3 magnetization plateau, which differs from the experimental behavior shown in Fig. 3(b). This qualitative difference is because the experimental results for $T < T_N$ reflect the magnetic order. In the ordered phase, the spin dynamics are described by the classical spins with continuous spin wave excitations, leading to the disappearance of the energy gap that causes the magnetization plateau. Similarly, the calculated magnetic susceptibility below T_N deviated significantly from the experimental result.

We examined the ground state of the spin-$\frac{1}{2}$ 2-4-coordinated lattice. Because J_{Cu} is stronger than the other interactions, the effective state of S_V-S_{Cu}-S_V trimer coupled by J_{Cu} is expected to become dominant and form a resultant spin of $S = 1/2$ as the temperature decreases. By further lowering the temperature, J_{V1} and J_{V2} contribute to the AF interactions between trimers, decreasing magnetic
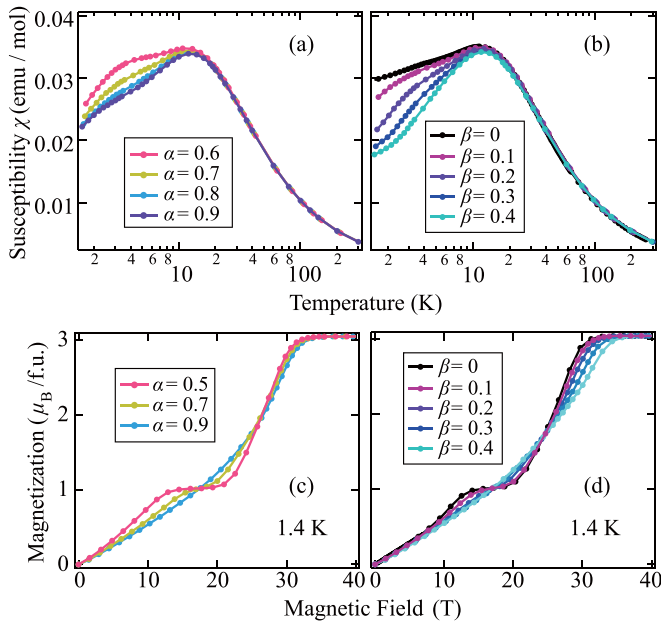
FIG. 4. Calculated magnetic susceptibilities for the spin-$\frac{1}{2}$ 2-4-coordinated lattice (a) with the representative values of α with fixed $\beta = 0.15$ and (b) with the representative values of β with fixed $\alpha = 0.70$. Calculated magnetization curves at 1.4 K for the spin-$\frac{1}{2}$ 2-4-coordinated lattice (c) with the representative values of α with fixed $\beta = 0.15$ and (d) with the representative values of β with fixed $\alpha = 0.70$.

susceptibility. If smaller values of α and β, i.e., weaker contributions from J_{V1} and J_{V2}, are assumed, the temperature where the AF correlations between trimers work effectively becomes lower. Therefore, the onset of significant decrease shifts to the lower temperature region, leading to a hump structure of magnetic susceptibility below the broad peak temperature, as shown in Figs. 4(a) and 4(b). By applying a magnetic field, the effective spin-$\frac{1}{2}$ state of the trimer becomes polarized along the field direction. Since a classical paramagnetic-like behavior describes the field-polarization process of weakly coupled spins, the linearity of the magnetization curve in the low-field region is enhanced as α and/or β decrease, as shown in Figs. 4(c) and 4(d). The subsequent 1/3 magnetization plateau corresponded to the full polarization of the effective spin-$\frac{1}{2}$ state of the trimer. The increase above the plateau phase toward saturation was considered to be associated with a change of the spin state of the trimer. This quantum description is expected to become more appropriate as the interactions between the trimers weaken. The calculated results indeed demonstrated the expansion of the quantum plateau region with decreasing α and β, as shown in Figs. 4(c) and 4(d).

Finally, we discussed the differences regarding the mechanisms of magnetization plateau by comparison with the spin-$(\frac{1}{2}, 1)$ Heisenberg 2-4-coordinated lattice in (p-Py-V-p-F)$_2$[Ni(hfac)$_2$] [23]. The AF interaction between 2- and 4-coordinated sites corresponds to J_{Ni} for (p-Py-V-p-F)$_2$[Ni(hfac)$_2$]. The 1/2 magnetization plateau in (p-Py-V-

p-F)$_2$[Ni(hfac)$_2$] is formed by the singlet dimer through J_{V1} and the full polarization of spin-1. Because J_{V1} is sufficiently large compared to the other AF interactions ($J_{Ni}/J_{V1} = 0.22$ and $J_{V2}/J_{V1} = 0.17$), the J_{V1} singlet dimer is stabilized with a large excitation energy gap, leading to the pronounced plateau width. For the present spin-$\frac{1}{2}$ 2-4-coordinated lattice, the 1/3 magnetization plateau corresponds to the full polarization of the spin-$\frac{1}{2}$ state of the trimer formed by J_{Cu}. The width of the plateau is considered to correspond mainly to an excitation energy gap between the effective spin-$\frac{1}{2}$ and -$\frac{3}{2}$ states of the trimer, resulting in strong α and β dependences, as shown in Figs. 4(c) and 4(d). The difference in magnitude between J_{Cu} and J_{V1} ($\alpha = 0.70$) is relatively small, leading to the relatively narrow plateau width in the present spin-$\frac{1}{2}$ 2-4-coordinated lattice.

V. SUMMARY

In this study, a verdazyl-based complex, (p-Py-V)$_2$[Cu(hfac)$_2$], was synthesized. MO calculations revealed that the three types of AF interactions formed a spin-$\frac{1}{2}$ 2-4-coordinated lattice. The experimental results for the specific heat C_p exhibited a sharp peak at $T_N = 3.6$ K, showing a phase transition to an ordered state owing to weak but finite interplane interactions. We observed an entire magnetization curve up to saturation. For $T > T_N$, the magnetization curve exhibited an almost linear increase in the low-field region, originating from the correlations in the 2-4-coordinated lattice. Furthermore, we observed a nonlinear increase in the high-field region, which demonstrated the reduction of the magnetic moment caused by the strong quantum fluctuations. We investigated the magnetic properties using the QMC method, and the magnetic susceptibility and magnetization curve for $T > T_N$ were explained well by the 2-4-coordinated lattice. We revealed that a hump structure of magnetic susceptibility is significantly related to the effective trimer state and the AF interactions between the trimers. Furthermore, the calculated magnetization curve exhibited a 1/3 magnetization plateau, which was not observed experimentally. This behavior was attributed to the full polarization of the effective spin-$\frac{1}{2}$ state of trimer. These results provide insight into unique quantum properties attributed to strong quantum fluctuations in the spin-$\frac{1}{2}$ 2-4-coordinated lattice. This study proposed a spin model with a mixed topology and will stimulate further research to understand unique quantum phenomena reflecting lattice topology.

[1] Z. Weihong, J. Oitmaa, and C. J. Hamer, Second-order spin-wave results for the quantum XXZ and XY models with anisotropy, Phys. Rev. B **44**, 11869 (1991).

[2] J. Oitmaa, C. J. Hamer, and Z. Weihong, Quantum magnets on the honeycomb and triangular lattices at $T = 0$, Phys. Rev. B **45**, 9834 (1992).

[3] E. V. Castro, N. M. R. Peres, K. S. D. Beach, and A. W. Sandvik, Site dilution of quantum spins in the honeycomb lattice, Phys. Rev. B **73**, 054422 (2006).

[4] H. C. Jiang, Z. Y. Weng, and T. Xiang, Accurate determination of tensor network state of quantum lattice models in two dimensions, Phys. Rev. Lett. **101**, 090603 (2008).

[5] K. Takano, Spin-gap phase of a quantum spin system on a honeycomb lattice, Phys. Rev. B **74**, 140402(R) (2006).

[6] W. Li, S.-S. Gong, Y. Zhao, and G. Su, Quantum phase transition, $O(3)$ universality class, and phase diagram of the spin-1/2 Heisenberg antiferromagnet on a distorted honeycomb lattice: A tensor renormalization-group study, Phys. Rev. B **81**, 184427 (2010).

[7] Y.-Z. Huang, B. Xi, X. Chen, W. Li, Z.-C. Wang, and G. Su, Quantum phase transition, universality, and scaling behaviors in the spin-1/2 Heisenberg model with ferromagnetic and antiferromagnetic competing interactions on a honeycomb lattice, Phys. Rev. E **93**, 062110 (2016).

[8] K. Uematsu and H. Kawamura, Randomness-induced quantum spin liquid behavior in the $s = 1/2$ Random J_1-J_2 Heisenberg antiferromagnet on the honeycomb lattice, J. Phys. Soc. Jpn. **86**, 044704 (2017).

[9] A. Kitaev, Anyons in an exactly solved model and beyond, Ann. Phys. (NY) **321**, 2 (2006).

[10] S. Trebst and C. Hickey, Kitaev materials, Phys. Rep. **950**, 1 (2022).

[11] Y. Motome and J. Nasu, Hunting majorana fermions in Kitaev magnets, J. Phys. Soc. Jpn. **89**, 012002 (2020).

[12] E. Manousakis, The spin-1/2 Heisenberg antiferromagnet on a square lattice and its application to the cuprous oxides, Rev. Mod. Phys. **63**, 1 (1991).

[13] A. W. Sandvik, Finite-size scaling of the ground-state parameters of the two-dimensional Heisenberg model, Phys. Rev. B **56**, 11678 (1997).

[14] H. Yamaguchi, K. Iwase, T. Ono, T. Shimokawa, H. Nakano, Y. Shimura, N. Kase, S. Kittaka, T. Sakakibara, T. Kawakami, and Y. Hosokoshi, Unconventional magnetic and thermodynamic properties of $S = 1/2$ spin ladder with ferromagnetic legs, Phys. Rev. Lett. **110**, 157205 (2013).

[15] H. Yamaguchi, H. Miyagai, M. Yoshida, M. Takigawa, K. Iwase, T. Ono, N. Kase, K. Araki, S. Kittaka, T. Sakakibara, T. Shimokawa, T. Okubo, K. Okunishi, A. Matsuo, and Y. Hosokoshi, Field-induced incommensurate phase in the strong-rung spin ladder with ferromagnetic legs, Phys. Rev. B **89**, 220402(R) (2014).

[16] H. Yamaguchi, T. Okubo, K. Iwase, T. Ono, Y. Kono, S. Kittaka, T. Sakakibara, A. Matsuo, K. Kindo, and Y. Hosokoshi, Various regimes of quantum behavior in an $S = 1/2$ Heisenberg antiferromagnetic chain with fourfold periodicity, Phys. Rev. B **88**, 174410 (2013).

[17] S. Miyamoto, Y. Iwasaki, N. Uemoto, Y. Hosokoshi, H. Fujiwara, S. Shimono, and H. Yamaguchi, Magnetic properties of honeycomb-based spin models in verdazyl-based salts, Phys. Rev. Mater. **3**, 064410 (2019).

[18] H. Yamaguchi, T. Okita, Y. Iwasaki, Y. Kono, N. Uemoto, Y. Hosokoshi, T. Kida, T. Kawakami, A. Matsuo, M. Hagiwara, Experimental realization of Lieb-Mattis plateau in a quantum spin chain, Sci. Rep. **10**, 9193 (2020).

[19] H. Yamaguchi, S. C. Furuya, S. Morota, S. Shimono, T. Kawakami, Y. Kusanose, Y. Shimura, K. Nakano, and Y. Hosokoshi, Observation of thermodynamics originating from a mixed-spin ferromagnetic chain, Phys. Rev. B **106**, L100404 (2022).

[20] H. Tsukiyama, S. Morota, S. Shimono, Y. Iwasaki, M. Hagiwara, Y. Hosokoshi, and H. Yamaguchi, Crystal structures and magnetic properties of verdazyl-based complexes with transition metals, Phys. Rev. Mater. **6**, 094417 (2022).

[21] S. Morota, Y. Iwasaki, M. Hagiwara, Y. Hosokoshi, and H. Yamaguchi, Magnetic anisotropy in a verdazyl-based complex with cobalt(II), J. Phys. Soc. Jpn. **92**, 054705 (2023).

[22] H. Yamaguchi, K. Shimamura, Y. Yoshida, A. Matsuo, K. Kindo, K. Nakano, S. Morota, Y. Hosokoshi, T. Kida, Y. Iwasaki, S. Shimono, K. Araki, and M. Hagiwara, Field-induced quantum phase in a frustrated zigzag-square lattice, Phys. Rev. Mater. **7**, L091401 (2023)

[23] Y. Tominaga, A. Matsuo, K. Kindo, S. Shimono, K. Araki, Y. Iwasaki, Y. Hosokoshi, S. Noguchi, and H. Yamaguchi, Mixed-spin two-dimensional lattice composed of spins 1/2 and 1 in a radical-Ni complex, Phys. Rev. B **108**, 024424 (2023).

[24] H. Yamaguchi, Y. Tominaga, A. Matsuo, S. Morota, Y. Hosokoshi, M. Hagiwara, and K. Kindo, Ladder-based two-dimensional spin model in a radical-Co complex, Phys. Rev. B **107**, 174422 (2023).

[25] R. Kuhn, Über Verdazyle und verwandte Stickstoffradikale, Angew. Chem. **76**, 691 (1964).

[26] M. C. Burla, R. Caliandro, M. Camalli, B. Carrozzini, G. L. Cascarano, L. De Caro, C. Giacovazzo, G. Polidori, and R. Spagna, SIR2004: an improved tool for crystal structure determination and refinement, J. Appl. Cryst. **38**, 381 (2005).

[27] G. M. Sheldrick: SHELXL97, Program for Crystal Structure Determination, University of Göttingen, Germany, 1997.

[28] M. Shoji, K. Koizumi, Y. Kitagawa, T. Kawakami, S. Yamanaka, M. Okumura, and K. Yamaguchi, A general algorithm for calculation of Heisenberg exchange integrals J in multispin systems, Chem. Phys. Lett. **432**, 343 (2006).

[29] A. W. Sandvik, Stochastic series expansion method with operator-loop update, Phys. Rev. B **59**, R14157 (1999).

[30] A. F. Albuquerque, F. Alet, P. Corboz, P. Dayal, A. Feiguin, L. Gamper, E. Gull, S. Gurtler, A. Honecker, R. Igarashi, M. Korner, A. Kozhevnikov, A. Lauchli, S. R. Manmana, M. Matsumoto, I. P. McCulloch, F. Michel, R. M. Noack, G. Pawlowski, L. Pollet *et al.*, The ALPS project release 1.3: Open-source software for strongly correlated systems, J. Magn. Magn. Mater. **310**, 1187 (2007).

[31] B. Bauer, L. D. Carr, A. Feiguin, J. Freire, S. Fuchs, L. Gamper, J. Gukelberger, E. Gull, S. Guertler, A. Hehn, R. Igarashi, S. V. Isakov, D. Koop, P. N. Ma, P. Mates, H. Matsuo, O. Parcollet, G. Pawlowski, J. D. Picon, L. Pollet *et al.*, The ALPS project release 2.0: Open source software for strongly correlated systems, J. Stat. Mech. Theory Exp. (2011) P05001.

[32] S. Morota, T. Kida, M. Hagiwara, Y. Shimura, Y. Iwasaki, and H. Yamaguchi, Magnetic properties of a spin-1/2 octagonal lattice, Phys. Rev. B **109**, 054401 (2024).

[33] F. J. Dyson, General theory of spin-wave interactions, Phys. Rev. **102**, 1217 (1956).

[34] J. Van. Kranendonk and J. H. Van Vleck, Spin waves, Rev. Mod. Phys. **30**, 1 (1958).

[35] A. S. T. Pires, Kosterlitz-Thouless transition in a two-dimensional isotropic antiferromagnet in a uniform field, Phys. Rev. B **50**, 9592 (1994).

[36] A. Cuccoli, T. Roscilde, R. Vaia, and P. Verrucchi, Field-induced XY behavior in the $S = 1/2$ antiferromagnet on the square lattice, Phys. Rev. B **68**, 060402(R) (2003).

[37] E. Čižmár, S. A. Zvyagin, R. Beyer, M. Uhlarz, M. Ozerov, Y. Skourski, J. L. Manson, J. A. Schlueter, and J. Wosnitza, Magnetic properties of the quasi-two-dimensional $S = 1/2$ Heisenberg antiferromagnet [Cu(pyz)$_2$(HF$_2$)]PF$_6$, Phys. Rev. B **81**, 064422 (2010).

[38] H. Yamaguchi, Y. Tamekuni, Y. Iwasaki, R. Otsuka, Y. Hosokoshi, T. Kida, and M. Hagiwara, Magnetic properties of a quasi-two-dimensional $S = 1/2$ Heisenberg antiferromagnet with distorted square lattice, Phys. Rev. B **95**, 235135 (2017).